Using SAGE on COTS UWB Signals for TOA Estimation and Body Shadowing Effect Quantification

Sander Coene
Department of Information Technology
Ghent University/IMEC
Ghent, Belgium
sander.coene@ugent.be

Cedric De Cock
Department of Information Technology
Ghent University/IMEC
Ghent, Belgium

Emmeric Tanghe
Department of Information Technology
Ghent University/IMEC
Ghent, Belgium

David Plets
Department of Information Technology
Ghent University/IMEC
Ghent, Belgium

Luc Martens
Department of Information Technology
Ghent University/IMEC
Ghent, Belgium

Wout Joseph
Department of Information Technology
Ghent University/IMEC
Ghent, Belgium

***Abstract*— This work assesses the applicability of the well-known SAGE algorithm for time-of-arrival estimation on ultra-wideband (UWB) measurements taken with cheap COTS hardware. Performance is comparable with a simple leading-edge detection (LDE) algorithm, establishing a general precision of approximately 30 cm/60 cm. SAGE performance is slightly worse in general (33 cm/71 cm), but is more stable in non-line-of-sight (NLOS) caused by human body presence. A more detailed breakdown of the effect of incidence angle on one-dimensional ranging accuracy is studied in relationship to human body shadowing effects. Within a cone of 135 degrees in front of the UWB device (pointing away from the body), the azimuthal incidence angle has no influence on the ranging performance of either algorithm.**

***Index Terms*—ultra-wideband, body shadowing, ranging, SAGE, WBANS, DecaWave, localization**

I. Introduction

Ultra-wideband (UWB) technology has the potential to provide indoor localization at cm-level accuracy with multipath tolerance at a low power consumption.

To fully leverage the wide bandwidth, academic research on UWB propagation characteristics and channel modeling is performed by using a Vector Network Analyzer (VNA), on which signals can be measured with a high sampling frequency – both in capture rate as well as resulting sampled signal bandwidth. The VNA, however powerful for research, is not suited as an end-user device, because of its prohibitive cost, size and power requirements.

Currently available commercial off-the-shelf (COTS) solutions for (end-user) UWB localization don't share the same characteristics. Commercial devices aim for a price-performance balance in a small, portable form-factor with low energy consumption, but are inherently outperformed by a VNA in terms of sampling frequency and spectral range.

Therefore it is important to not limit application of academic research to high-quality VNA data, but also investigate its applicability on measurements performed with COTS solutions.

In 2013, the company DecaWave (DW) brought an UWB chipset and antenna to market, the DW1000 [1], which since has been the choice of many researchers looking for an affordable and accurate localization solution [2]. In recent years, this has enabled advancements in new ranging schemes and algorithms, trying to squeeze as much as possible out of such a COTS platform. Corbalan [3] and Grosswindhager [4] have investigated concurrent ranging, side-stepping a low-resolution transmission timer. However, the same cannot be said on the multipath estimation side. Adaptive leading-edge detection (LDE) [5] and superresolution algorithms like SAGE [6] and MUSIC [7] to perform the first-path detection are almost exclusively applied to VNA data or synthetic channels [8]–[13]. This means that the performance gain on COTS systems is not clear and left to the imagination of the reader. This lack of data on lower-cost chipsets and hardware designs is a clear shortcoming on the road to UWB for handheld end-user devices. This paper bridges this gap by applying an LDE and a SAGE algorithm, on measurements done with the DW system.

Additionally, in some scenarios one part of a pair of ranging devices can be located in the vicinity of the human body, as part of a so-called wireless body area network (WBAN). As the human body affects RF signal propagation, the signal can experience attenuation and/or dispersion depending on the path taken between sender (TX) and receiver (RX). This effect has already been investigated in [14], [15], the latter reporting an attenuation of up 18 dB, leading to a ranging error of up to 60 cm. This clearly has an effect on the localisation accuracy as well, and [16] reports a 3D localisation P90 error of up to 4 m for a device attached to the chest, up from 21 cm for a

tripod-mounted solution.

While an interesting observation, the use of 3D localisation to report the human body shadowing effect obscures the effect on one-dimensional (1D) ranging. 3D localisation is a higher-level process using multiple signals that inherently compensates these errors up to a certain level.

Here we therefore propose a more in-depth analysis of the 1D ranging accuracy, to chart the weaknesses of time-of-arrival (TOA) algorithms with respect to the incidence angle.

Concretely the novelty of this paper is twofold: i) performance comparison of SAGE and LDE algorithms on COTS hardware; ii) quantification of human body shadowing effect on COTS measurements with detailed incidence angle breakdown.

The remainder of this paper presents the measurement setup used to obtain the data (section II), a short description on the algorithms used to obtain a ranging estimate (section III), followed by a discussion of the results (section IV) and conclusions, including ideas for future research (section V).

II. Measurement setup

This section describes the measurement equipment and environment used to obtain the data.

A. Hardware

The DecaWave DW1000 platform is chosen as COTS transceiver solution. This IEEE802.15.4-2011 compliant chipset has a chipping rate of 499.2 MHz and supports six radiofrequency (RF) bands (UWB band 1–5, 7), spanning from 3.5 GHz to 6.5 GHz. With a sampling clock of 63.8976 GHz, the message timestamp resolution[1] is about 15.65 ps.

The DW chip performs a 1D ranging estimate using a leading-edge detection (LDE) algorithm (see subsection III-A) on the channel impulse response (CIR) [17]. Ranging errors of under 10 cm have been reported [2]. The implementation details of the LDE algorithm on the chip have not been published. The measured CIR is stored as a series of complex values in one of the registers. Each point in time represents a time-sample of about 1.0016 ns.

The measurement data are taken from a specialized anchor-tag solution, developed in [18]. The DW transceiver is placed on a custom UWB add-on board and combined with a sub-GHz IoT platform, the Zolertia Re-Mote. An SMA connector attaches a planar dipole antenna.

A two-way ranging (TWR) scheme is used to force communication of a tag (representing an end-user) and an anchor (the fixed infrastructure). The tag initializes the TWR distance estimate and both the estimate and the CIR – as well as some diagnostic information – are retrieved through a wired USB connection from the tag.

[1]For scheduled sending, there is up to 8 ns timing jitter. The timestamp itself is still accurate.

B. Environment

Figure 1 shows the open indoor area measurement considered here [19]. The rectangular windowless room with concrete walls measures 50 m-by-11 m and features an open central area with three rows of metal shelves in the back. The ceiling is approximately 2.5 m high with metal rails to support electrical cabling and lights.

The room has motion capture system, which uses ten infra-red cameras and reflective tracker spheres, to construct the ground truth of object locations and orientations in six dimensions. The expected accuracy of this system is well below centimetre-level for the performed measurements.

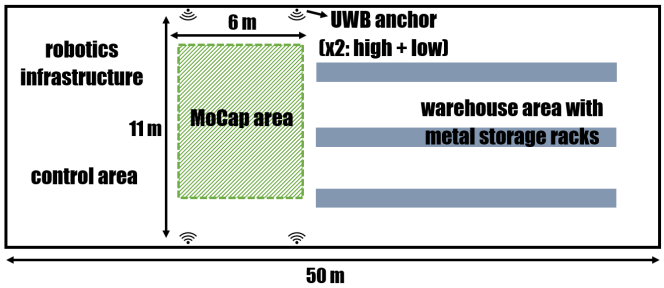

Figure 1. Ground plan of the IIoT lab, measurements take place in the area designated as 'MoCap area'.

The measurements are done in the rectangular central area of 6 m by 11 m with the specialized DW device (as described in subsection II-A). In each of the corners two DW anchors are placed at different heights, defining a cube of roughly 6 m-by-11-by-2.5 m with eight anchors in total. To stay within range of all infrared cameras, the extremes of this cube are avoided.

For the first dataset, the receiving device (tag) is placed on a camera mounting pole, at average male chest height (1.5 m). A set of reflective markers on the antenna enable the ground truth position acquisition. Measurements are taken at three different locations, with rotation changing in 45° increments. Per position/rotation pair, two sets of data are retrieved: a 'baseline CIR' and an 'body CIR'. The former consists of the mounted tag, with nothing in the central area. The latter emulates a user-wearable tag, with a human male standing next to the pole-mounted tag. The user-tag distance therefore fluctuates slightly across measurements. This is the case as well for real-world applications, thus not a threat to the research outcomes of this paper. Per configuration (location/rotation/human presence) multiple points are obtained.

The second dataset focuses on the effect of incidence angle, with locations spread across the room. The tag is now fixed to a cardboard mounting solution placed at pelvis height on a male researcher (the user) of average build and height. Reflective markers are added to the cardboard pane to ensure good visibility for the infrared tracking. Placement of the solution on both the front and back side is considered, to simulate placement of an UWB solution in the front or back pocket.

Both measurements are performed in a static way, i.e. both the environment and the tag remain immobile, small movements of the human body notwithstanding. The tag initiates a TWR conversation between all eight anchors consecutively.

Table I lists the UWB device settings for the different datasets used in section IV.

Table I
MEASUREMENT SETTINGS

Dataset nr.	Settings			
	Channel	PRF (MHz)	Bitrate (kb/s)	Preamble length
1	3	64	850	512
2	5	64	850	1024

C. Signal pre-processing

To apply different algorithms and compare them to the COTS hard- and software platform, the channel impulse response (CIR) needs to be extracted from the DW1000.

The channel measurement takes place between two independent devices. Even though the sub-GHz backbone takes care of clock synchronisation, the phase is incoherent, i.e. it can not be used for absolute time-of-arrival estimation.

Additional caveat is the CIR itself, which consists of 1016 complex samples in the time domain with step size of $\Delta t \approx 1.0016$ ns.

To start the accumulation of the message pre-amble, the chipset makes an initial guess of what part of the signal constitutes the direct path using signal intensity. This first direct path estimate is likely to be an overestimation: when the direct path is attenuated because of obstacles, there can be reflected multipath components – with a longer travel time – which have a higher signal intensity. This is accounted for by the chipset.

The DecaWave chipset subsequently performs a ranging estimation. It identifies the CIR bin (and fractional part) corresponding to the direct path and connects this with the UWB message, timestamped for calculation of the time of flight. From this, a range estimate is given.

Because of this behaviour, it is impossible to directly run a TOA algorithm on the CIR data to compare ranging results. Therefore, a time series t is generated using (1), based on the first path bin index i_{FP} and time of flight calculated from the TWR distance estimate d_{FP}. Here, $\Delta t = 1/(2 \cdot 499.2\ \text{MHz})$ is defined by the chipping rate, with $i = 1 \dots 1016$ the index of the timeseries and c the speed of light (in air).

$$t(i) = \Delta t \cdot (i - i_{FP}) + \frac{d_{FP}}{c} \tag{1}$$

Since no additional information on possible clock drift is available to algorithms run externally, they are at a (minor) disadvantage. TWR schemes apply corrections to account for the processing time on the anchor, which contributes to the round trip time for a message, but is not part of the time of flight. With this approach, there is the implicit expectation that this contribution is already filtered out and the algorithm can work as it would for a completely synchronised one-way ranging scheme.

III. TIME OF ARRIVAL ALGORITHMS

A. LDE

The leading-edge detection (LDE) algorithm makes use of window functions to filter the signal and construct a more dynamic threshold detector. This paper follows a partial implementation details of [20], leaving out the adaptive portion of the algorithm. This corresponds, according to [20], to the max-ratio LDE algorithm of [21]. For clarity, a different notation is used for the functions.

The CIR is represented by $h(t)$, with t sampled at discrete, fixed-interval points in time. As a first step, the CIR h is upsampled using the built-in MATLAB function `interp` with an upsampling factor of 20.

$$y(t) = w_{\text{average}}\left(|h(t)|, N_{\text{average}}\right) \tag{2}$$

Equation (2) applies an averaging window to the absolute value of the CIR, using a window size of N_{average} points. Though seemingly working against the initial upsampling of the CIR, the combination of averaging on top of upsampling has proven beneficial.

$$u(t) = w_{\text{max}}\left(y(t), N_{\text{max1}}\right) \tag{3}$$

$$v(t) = w_{\text{max}}\left(y(t), N_{\text{max2}}\right) \tag{4}$$

Equations (3) and (4) apply a max-window function to the averaged CIR data y, using a window size of N_{max1} and N_{max2} points, respectively.

$$r(t) = (\alpha \cdot u(t) > v(t)) \wedge (v(t) > \Theta_{\text{thr}}) \tag{5}$$

$$\Theta_{\text{thr}} = \beta \cdot \mu_{\text{noise}} + \gamma \cdot \sigma_{\text{noise}} \tag{6}$$

A binary ratio check is performed using (5), where the logical value r indicates the presence of a leading edge, with α a fixed multiplier. The threshold value Θ_{thr} is defined by (6), using the noise statistics from the CIR, the mean μ_{noise} and the standard deviation σ_{noise}, multiplied by fixed factors β and γ, respectively. This differs slightly from [20], as the threshold here is completely determined by the noise, without the proposed additional, manually-set threshold. Note that the noise statistics are calculated from a truncated set of CIR points. Because of the limited size of the extracted CIR, only the first 15 ns worth of signal are considered as noise.

Table II contains the LDE algorithm parameters, as used for the different ranging error datasets presented in this paper.

Table II
LDE ALGORITHM PARAMETERS

Dataset nr.	Parameters					
	N_{average}	N_{max1}	N_{max2}	α	β	γ
1	16	16	256	8.0	4.0	4.4
2	16	16	256	8.0	4.0	4.4

As mentioned before, the algorithm is applied to an upsampled CIR, with factor 20. This leads to a lowest possible precision of approximately 1.5 cm.

B. SAGE

The Space Alternating Generalised Expectation Maximisation (SAGE) algorithm is an extension of the Expectation Maximisation (EM) algorithm, which uses maximum-likelihood estimation (MLE) to obtain a signal reconstruction. From the individual paths that are reconstructed, information on the signal propagation can be extracted, and with it, the first path immediately leads to an estimate of the TOA and therefore the distance. The algorithm has been extensively studied in literature [6], [8], [14], [22]–[24]. Additionally, [12] has already studied the influence of the human body and a mitigation technique using a modified signal model. This paper follows the implementation details and notation of [9], though with a sole focus on TOA estimation, rather than joint TOA/AOA estimation. With this simplification, the lack of additional dimensions reduces the SAGE algorithm in essence to the EM algorithm it is based on.

Equation (7) describes the received signal $Y(t)$ as a finite collection of L plane waves impinging on the antenna. This superposition of waves is corrupted by white Gaussian noise $N(t)$. N_0 is a positive constant. One wave or multipath component (MPC) l is defined by its parameters θ_l, such that all wave parameters are contained within $\theta \triangleq [\theta_1, \ldots, \theta_L]$. For a single-antenna system, an MPC is only defined by a relative delay τ_l and a complex amplitude α_l. This information is represented by $\theta_l = [\tau_l, \alpha_l]$.

$$\begin{aligned} Y(t) &= \sum_{l=1}^{L} s(t;\theta_l) + \sqrt{\frac{N_0}{2}} N(t) \\ &= s(t;\theta) + \sqrt{\frac{N_0}{2}} N(t) \end{aligned} \tag{7}$$

Equation (8) gives the l-th wave's contribution contained within $s(t;\theta_l)$. The function $p(t)$ represents a single UWB pulse in the baseband.

$$s(t;\theta_l) = \alpha_l \, p(t - \tau_l) \tag{8}$$

Equation (9) introduces the complete but unobservable data $X_l(t)$, for each wave, from which the observable (but incomplete) data $Y(t)$ is constructed. From this follows (10).

$$X_l(t) = s(t;\theta_l) + \sqrt{\frac{N_0}{2}} N_l(t) \tag{9}$$

$$Y(t) = \sum_{l=1}^{L} X_l(t) \tag{10}$$

The goal of the algorithm is to provide an estimate $\hat{x}_l$ of $X_l(t)$ given an observation $y(t)$ and a previous estimate of the parameter vector $\hat{\theta}'$. The conditional expectation in (11) lends its name to this part of the algorithm: the Expectation (E) step.

$$\hat{x_l}(t;\hat{\theta}') \triangleq \mathrm{E}_{\hat{\theta}'} \left\{ X_l(t) \,|\, y(t) \right\} \tag{11}$$

Equation (12) estimates the complete data for the l-th MPC using the observation y by subtracting all other wave contributions from it.

$$\hat{x_l}(t;\hat{\theta}') = y(t) - \sum_{l'=1, l' \neq l}^{L} s(t;\hat{\theta}'_{l'}) \tag{12}$$

Next, the Maximisation (M) step is performed. A new estimate of the delay time is obtained using (13), while (14) computes a new complex amplitude. The cost function z is given by (15).

$$\hat{\tau_l}'' = \arg\max_{\tau} \left\{ \left| z\left(\tau; \hat{x_l}(t;\hat{\theta}')\right) \right| \right\} \tag{13}$$

$$\hat{\alpha_l}'' = \frac{z\left(\hat{\tau}''; \hat{x_l}(t;\hat{\theta}')\right)}{\int_0^T |p(t - \hat{\tau_l}'')|^2 \, dt} \tag{14}$$

$$z\left(\tau; x_l\right) \triangleq \int_0^T p^H(t' - \tau) x_l(t') \, dt' \tag{15}$$

Algorithm success largely depends on the chosen parameters: the search space (and resolution) of the M step for each parameter (τ_i), the number of MPCs L to decompose the signal into, as well as the number of iterations to try to achieve convergence.

Since we focus on time of arrival estimation, a complete channel parameter estimation is not needed. Therefore, TOA search space can be limited to the window up to and including the maximum power wave (i.e. highest magnitude peak in the CIR). A limited number of MPCs (15-25) suffices then to capture the direct path, discarding noisy paths using a power comparison. Similarly, a low number of iterations is enough to yield satisfactory convergence. Table III presents the values as used on the different datasets.

Table III
SAGE ALGORITHM PARAMETERS

Dataset nr.	**Parameters**	
	MPCs to estimate	number of iterations
1	25	1
2	30	1

Note that because SAGE models the signal as a superposition of plane waves, upsampling the obtained CIR does not make sense without changing the signal model. This limits the possible precision of the implementation of the algorithm as presented here to approximately 30 cm, in line with the CIR time bin width. Despite this disadvantage, it is still possible to draw conclusions in terms of relative performance, keeping this limitation in mind.

IV. Results

A. Algorithm ranging performance comparison

Dataset 1 contains 5945 data points, with a ground truth (section II). Both algorithms provide a ranging estimate, which is compared to this ground truth. Figure 2 shows the error using a cumulative distribution function (CDF). The limited precision possible with SAGE algorithm (lack of subsampling) explains the flatter slope around 0 m, and is indeed around 30 cm wide.

The shoulder, where the vertical slope tapers off to a more horizontal line on the right half of the graph, is bit higher for the SAGE curve (at the 92th percentile) than for the LDE curve (at the 85th percentile). This indicate a slightly better performance of the SAGE algorithm. Inversely, this is compensated by its tendency to underestimate the range in some cases (i.e. identify noise as a MPC, as seen in the tail towards the left side of the graph). Both algorithm behave similarly in terms of over significant overestimation (more or less same sloping behavior for ranging errors higher than 0.5 m). Maximum errors are the same for both, at around 2 m (not shown on graph).

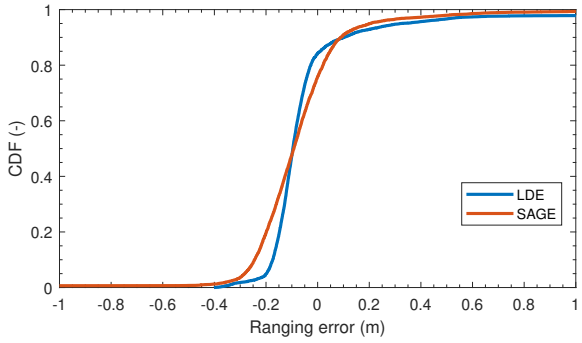

Figure 2. CDF of the ranging error for LDE and SAGE algorithm on dataset 1.

Since dataset 1 consists of both measurements in the absence and presence of the human body, Figure 3 shows the ranging error CDF for both cases separately. This dataset contains 5130 data points. As the body measurements contain datapoints corrupted by signal attenuation of through-body propagation (or creeping waves around the body), it is evident, that the presented algorithms perform better on the baseline measurement. It must be noted that for the baseline measurements, the LDE algorithm barely has an edge over the SAGE algorithm, keeping again in mind the inherent lower precision of SAGE. The graph of the body measurements shows the origin of the higher shoulder for SAGE that is also present when looking at the total performance in Figure 2.

Figure 4 shows the CDF for dataset 2, in which the tag is always attached to the human user, and therefore more likely to experience the influence of its body influence. The shoulder for both algorithms is significantly lower than for dataset 1, even when looking only at body measurements. The difference in slope angle between LDE and SAGE remains similar, and again, the SAGE shoulder starts slightly higher than of its

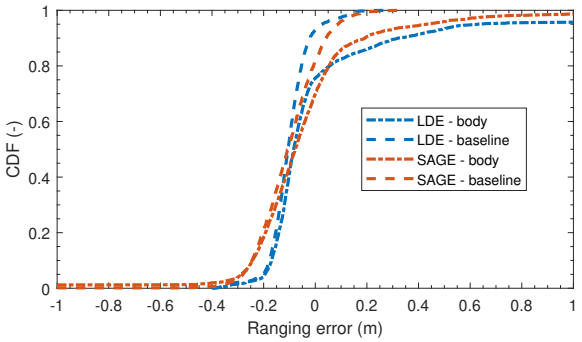

Figure 3. CDF of the ranging error for LDE and SAGE algorithm on dataset 1, evaluating baseline and body measurements separately.

competitor. It is however lower than before, and therefore does not indicate better performance as earlier, giving the edge to the LDE algorithm.

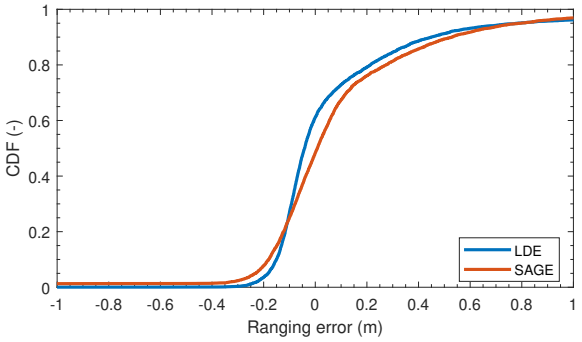

Figure 4. CDF of the ranging error for LDE and SAGE algorithm on dataset 2, in presence of human body.

Some ranging algorithms introduce a bias to the estimation they provide (e.g. identifying slope rather than peak of a wave). This reduces the accuracy and can hinder a neutral comparison between results. Therefore, using the error of the Xth percentile P_X would not be a good figure of merit. Even more so since the error can become negative when an algorithm underestimates the distance. Therefore, by subtracting the 10th percentile P_{10} from the 90th P_{90}, we obtain the difference in ranging error percentiles $\Delta P = P_{90} - P_{10}$, which provides a better metric to compare performance than isolated percentile values.

Another metric that can be used is the Cramer-Rao lower bound (CRLB). First, the CDF of the ranging error is approximated by a Gaussian mixture model. From this, the CRLB is calculated based on a theoretical model. This metric is similarly not affected by bias.

Table IV presents both metrics for the different datasets. The ΔP shows that both algorithms have a precision of around 30 cm (dataset 1) up to 71 cm (dataset 2). The LDE algorithm establishes a slightly better result overall, in both ΔP and CRLB. Interestingly enough, comparing baseline versus body measurements, LDE suffers a increase in spread of 313%, whereas SAGE's spread increases by approximately half that,

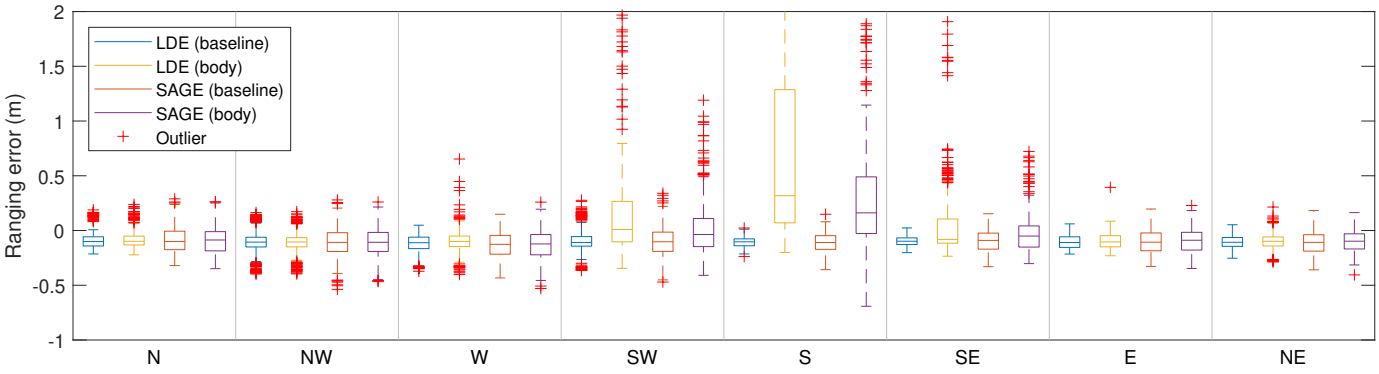

(a) Ranging statistics

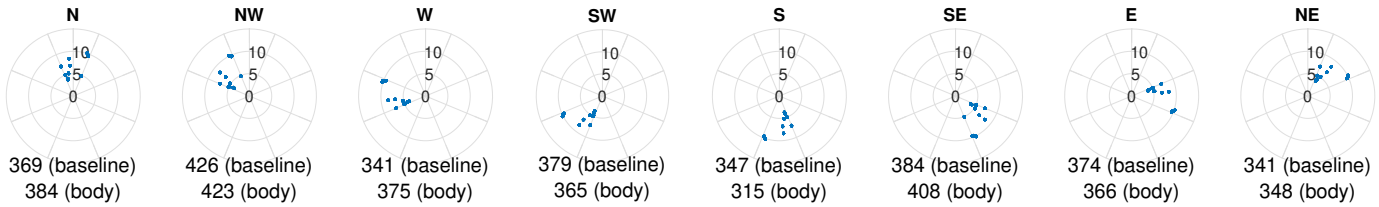

(b) Measurement data point amount and distribution; radial axis in (m)

Figure 5. Ranging errors for dataset 1, grouped by perceived incidence angle (expressed in cardinal and ordinal compass directions). The box plots are created using the 25th and 75th percentile. The incidence angle is taken from the relative coordinate system of the tag, where North (N) points away from the user (where applicable). Looking down from the ceiling determines the counter-clockwise compass layout. For South (S) incidence, the signal has to travel through or around the body.

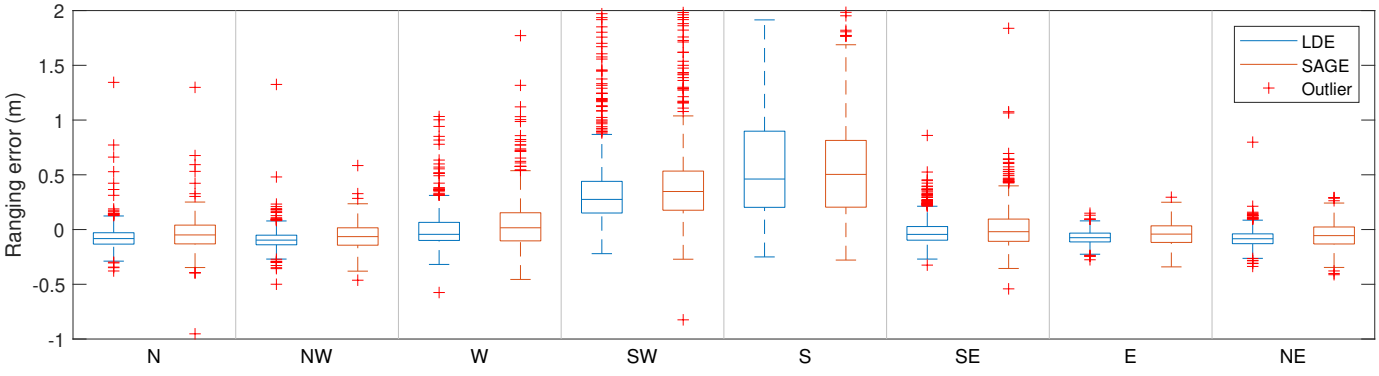

(a) Ranging statistics

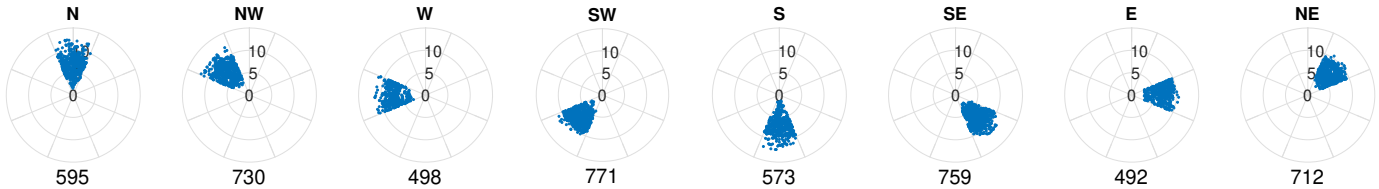

(b) Measurement data point amount and distribution; radial axis in (m)

Figure 6. Ranging errors for dataset 2, grouped by perceived incidence angle (expressed in cardinal and ordinal compass directions). The box plots are created using the 25th and 75th percentile. The incidence angle is taken from the relative coordinate system of the tag, where North (N) points away from the user. Looking down from the ceiling determines the counter-clockwise compass layout. For South (S) incidence, the signal has to travel through or around the body.

at 152%. CRLB figures are up by 43% for both algorithms.

Table IV
ALGORITHM PERFORMANCE METRICS OF DIFFERENT DATASETS

Data-set nr.	LDE		SAGE	
	ΔP (m)	CRLB (cm)	ΔP (m)	CRLB (cm)
1	0.278	0.4	0.334	1.5
1 (baseline)	0.157	0.35	0.287	1.30
1 (body)	0.492	0.50	0.437	1.86
2	0.599	0.9	0.712	2.5

It should again be noted that the SAGE algorithm as presented in the figures does not estimate smaller than the timestep, and is as such restricted to a precision of approximately 30 cm (distance traveled by light in the Δt of 1 ns). Therefore, the spread of approximately 33 cm is not surprising and close to the lower error limit.

As it stands, the LDE algorithm is better suited for the COTS measurements of lower resolution. Both performance (and execution time, not further discussed here) are better than with the SAGE algorithm. There is potential for SAGE when adjusted to the coarser sampling of COTS hardware. Using a signal model that models the complete data as an UWB pulse rather than a Dirac pulse can help. This has been performed successfully in a different context (not using SAGE) in [25].

B. Human body influence

It is obvious that the human body can contribute to poor signal quality, by deforming and attenuating the electromagnetic fields. This in turn lowers the possible ranging accuracy for any algorithm.

Fig. 5(a) shows an indication of the precision and accuracy of the ranging accuracy in function of the angle for dataset 1. For statistical reasons, each measurement point is assigned to an octant area (spanning 45 degrees), depending on the angle of incidence. This angle is measured relative to the tag mounted on the user. 0 degrees (North) points away from the user, meaning that the signal can reach the receiver with a direct line-of-sight (LOS) (since no other obstacles can block the signal in the measurement environment). 180 degrees (South) points towards the user, such that the signal must travel through (or around) the body to reach the receiver. This situation is called non-line-of-sight (NLOS). Four graphs show the relationship between the algorithm performance and the presence of the human body. Unsurprisingly for the baseline measurement, there is no real impact with changing incidence octant. For the body measurements, both the precision and accuracy worsen.

The LDE algorithm median increases by 42 cm from best case (N) to worst case (S), indicating a much higher tendency to overestimate the time of flight, when the signal traverses the human body. Its inter-percentile distance between P_{75} and P_{25} increases similarly from 8 cm up to 1.21 m.

The SAGE algorithm seems more robust towards this change in incidence angle, with the median increasing only 25 cm. Its inter-percentile distance increases from 18 cm to 51 cm, which is a modest increase of 183% when compared to the 1413% increase of the LDE algorithm.

Fig. 5(b) shows the corresponding measurements of dataset 1 in the local coordinate system of the tag.

Figure 6 shows similar statistics for dataset 2, where the human body is always present. Here both algorithms perform worse, but the decrease in both accuracy and precision with increased body traversal is less outspoken. This can be explained by a more uniform distribution of distance and incidence angle, whereas dataset 1 might unintentionally emphasize situations in which LDE generally performs worse than SAGE.

For dataset 2, LDE's median increases by 54 cm, while its inter-percentile distance increases from 10 cm to 70 cm (+600%). SAGE's median increases by 55 cm, while its inter-percentile distance increases from 17 cm to 61 cm (+259%). Again, SAGE is modestly better suited for NLOS conditions.

Both figures 5(a) and 6(a) establish a 'cone of ignorance', as the ranging performance barely changes across octants E, NE, N and NW. As such, this cone has an angle of 135 to 180 degrees. The cone is slightly wider for dataset 1, the distance between the user and UWB is a bit larger. This allows more waves to come in from the sides of the user without hindrance.

According to literature [12], it is possible to simulate the resulting field deformation near the human. A modified signal model based on the simulated field deformations can be used to improve the SAGE algorithm. This is not yet attempted in this work. If applied in conjunction with the UWB pulse shape for signal decomposition, SAGE might be worth the additional calculation time.

V. CONCLUSIONS AND FUTURE WORK

The SAGE algorithm, while a good choice for high-resolution data obtained with a VNA, has only average performance on COTS hardware like the DW1000 transceiver. In general it is outperformed by the much simpler LDE algorithm, in both speed and performance (90-10th percentile precision of 28/60 cm vs 33/71 cm; dataset 1/2, LDE vs SAGE). A redeeming factor is its better behavior in NLOS situations, suffering only a 259% increase in ranging error spread, as opposed to the 600% of the LDE algorithm (75-25th percentile precision of 121/70 cm vs 51/61 cm; dataset 1/2, LDE vs SAGE). There still exists an opportunity for increased accuracy by combining a modified signal model [12], [25] into SAGE that more accurate simulates the UWB pulse as captured by COTS hardware. Additionally, dynamical modifications with changing on-body position and incidence angle should also be possible.

The attenuation of the signal in vicinity of a human body and its effect on ranging accuracy lie in line with other research. The more detailed breakdown of the human body effect described here does add opportunities for more fine-tuned mitigation techniques. This can be achieved on either the ranging level (e.g. SAGE with modified signal model)

or higher-level localisation techniques (e.g. anchor selection, ranging error weighting).

Future work will consist of optimising the SAGE algorithm for ranging instead of channel characterisation, with a focus on near-body scenarios. While normally used for offline evaluation, we hope to implement enough modifications to run the algorithm in real-time to enable its use in embedded solutions.

ACKNOWLEDGMENT

The authors would like to thank E. De Poorter, B. Van Herbruggen and N. Macoir from IDLab Ghent for their support on the DW measurements.

REFERENCES

[1] DecaWave, "DecaWave Launches Industry's Most Precise Indoor Location and Communication CMOS Chip," Nov. 2013.

[2] A. R. Jimenez Ruiz and F. Seco Granja, "Comparing Ubisense, BeSpoon, and DecaWave UWB Location Systems: Indoor Performance Analysis," *IEEE Transactions on Instrumentation and Measurement*, vol. 66, no. 8, pp. 2106–2117, Aug. 2017.

[3] P. Corbalán and G. P. Picco, "Concurrent ranging in ultra-wideband radios: Experimental evidence, challenges, and opportunities," in *Proceedings of the 2018 International Conference on Embedded Wireless Systems and Networks*, ser. EWSN '18. USA: Junction Publishing, 2018, pp. 55–66.

[4] B. Großwindhager, M. Stocker, M. Rath, C. A. Boano, and K. Römer, "SnapLoc: An ultra-fast UWB-based indoor localization system for an unlimited number of tags," in *Proceedings of the 18th International Conference on Information Processing in Sensor Networks*. Montreal Quebec Canada: ACM, Apr. 2019, pp. 61–72.

[5] M. J. Kuhn, J. Turnmire, M. R. Mahfouz, and A. E. Fathy, "Adaptive leading-edge detection in UWB indoor localization," in *2010 IEEE Radio and Wireless Symposium (RWS)*. New Orleans, LA, USA: IEEE, Jan. 2010, pp. 268–271.

[6] B. Fleury, D. Dahlhaus, R. Heddergott, and M. Tschudin, "Wideband angle of arrival estimation using the SAGE algorithm," in *Proceedings of ISSSTA'95 International Symposium on Spread Spectrum Techniques and Applications*, vol. 1. Mainz, Germany: IEEE, 1996, pp. 79–85.

[7] H. Dropkin and C. Ly, "Superresolution for scanning antenna," in *Proceedings of the 1997 IEEE National Radar Conference*, May 1997, pp. 306–308.

[8] K. Haneda and J. Takada, "High-resolution estimation of NLOS indoor MIMO channel with network analyzer based system," in *14th IEEE Proceedings on Personal, Indoor and Mobile Radio Communications, 2003. PIMRC 2003.*, vol. 1, Sep. 2003, pp. 675–679 Vol.1.

[9] K. Hausmair, K. Witrisal, P. Meissner, C. Steiner, and G. Kail, "SAGE algorithm for UWB channel parameter estimation," COST2100, Athens, Greece, 10th Management Committee Meeting TD(10)10074, Feb. 2010.

[10] P. J. Chung and J. F. Böhme, "DOA estimation using fast EM and SAGE algorithms," *Signal Processing*, vol. 82, no. 11, pp. 1753–1762, Nov. 2002.

[11] M. Matthaiou, D. I. Laurenson, N. Razavi-Ghods, and S. Salous, "Characterization of an Indoor MIMO channel in Frequency Domain using the 3D-SAGE Algorithm," in *2007 IEEE International Conference on Communications*. Glasgow, Scotland: IEEE, Jun. 2007, pp. 5868–5872.

[12] S. Van Roy, L. Liu, C. Oestges, and P. De Doncker, "An ultra-wideband SAGE algorithm for body area networks," in *2009 International Conference on Electromagnetics in Advanced Applications*. Torino, Italy: IEEE, Sep. 2009, pp. 584–587.

[13] O. P. Pasquero and R. D'Errico, "A Spatial Model of the UWB Off-Body Channel in Indoor Environments," *IEEE Transactions on Antennas and Propagation*, vol. 64, no. 9, pp. 3981–3989, Sep. 2016.

[14] N. Amiot, M. Mhedhbi, B. Uguen, and R. DErrico, "WBAN Off-Body channel angular structure comparison between SAGE estimation and ray tracing simulation," in *2015 9th European Conference on Antennas and Propagation (EuCAP)*, 2015, pp. 1–5.

[15] T. Otim, A. Bahillo, L. E. Diez, P. Lopez-Iturri, and F. Falcone, "FDTD and Empirical Exploration of Human Body and UWB Radiation Interaction on TOF Ranging," *IEEE Antennas and Wireless Propagation Letters*, vol. 18, no. 6, pp. 1119–1123, Jun. 2019.

[16] T. Otim, L. E. Díez, A. Bahillo, P. Lopez-Iturri, and F. Falcone, "Effects of the Body Wearable Sensor Position on the UWB Localization Accuracy," *Electronics*, vol. 8, no. 11, p. 1351, Nov. 2019.

[17] DecaWave, *DW1000 User Manual v2.18*, 2017.

[18] B. Van Herbruggen, B. Jooris, J. Rossey, M. Ridolfi, N. Macoir, Q. Van den Brande, S. Lemey, and E. De Poorter, "Wi-PoS: A Low-Cost, Open Source Ultra-Wideband (UWB) Hardware Platform with Long Range Sub-GHz Backbone," *Sensors*, vol. 19, no. 7, p. 1548, Mar. 2019.

[19] "Industrial IoT Lab," https://www.ugent.be/ea/idlab/en/research/research-infrastructure/industrial-iot-lab.htm.

[20] M. J. Kuhn, J. Turnmire, M. R. Mahfouz, and A. E. Fathy, "Adaptive leading-edge detection in UWB indoor localization," in *2010 IEEE Radio and Wireless Symposium (RWS)*. New Orleans, LA, USA: IEEE, Jan. 2010, pp. 268–271.

[21] B. C. Merkl, "The Future of the Operating Room: Surgical Preplanning and Navigation using High Accuracy Ultra-Wideband Positioning and Advanced Bone Measurement," Ph.D. dissertation, University of Tennessee - Knoxville, Dec. 2008.

[22] M. Tschudin, R. Heddergott, and P. Truffer, "Validation of a high resolution measurement technique for estimating the parameters of impinging waves in indoor environments," in *Ninth IEEE International Symposium on Personal, Indoor and Mobile Radio Communications (Cat. No.98TH8361)*, vol. 3. Boston, MA, USA: IEEE, 1998, pp. 1411–1416.

[23] K. Haneda, J. Takada, and T. Kobayashi, "Experimental evaluation of a SAGE algorithm for ultra wideband channel sounding in an anechoic chamber," in *2004 International Workshop on Ultra Wideband Systems Joint with Conference on Ultra Wideband Systems and Technologies. Joint UWBST & IWUWBS 2004 (IEEE Cat. No.04EX812)*. Kyoto, Japan: IEEE, 2004, pp. 66–70.

[24] B. Fleury, M. Tschudin, R. Heddergott, D. Dahlhaus, and K. Ingeman Pedersen, "Channel parameter estimation in mobile radio environments using the SAGE algorithm," *IEEE Journal on Selected Areas in Communications*, vol. 17, no. 3, pp. 434–450, Mar. 1999.

[25] J. Kulmer, S. Hinteregger, B. Grosswindhager, M. Rath, M. S. Bakr, E. Leitinger, and K. Witrisal, "Using DecaWave UWB transceivers for high-accuracy multipath-assisted indoor positioning," in *2017 IEEE International Conference on Communications Workshops (ICC Workshops)*. Paris, France: IEEE, May 2017, pp. 1239–1245.